IEEE Access
Multidisciplinary ⋮ Rapid Review ⋮ Open Access Journal

Received 5 March 2026, accepted 17 March 2026. Date of publication 00 xxxx 0000, date of current version 00 xxxx 0000.

Digital Object Identifier 10.1109/ACCESS.2026.3676282

Hand-Guided Human–Robot Interaction With a Learning-Based Controller for Soft Robot Arms

DANIELE SOMMA[1,2], (Graduate Student Member, IEEE), DIEGO BIANCHI[1,2], (Student Member, IEEE), FRANCESCO IORI[1,2], CECILIA LASCHI[3,4], (Fellow, IEEE), AND EGIDIO FALOTICO[1,2], (Member, IEEE)

[1]The BioRobotics Institute, Scuola Superiore Sant'Anna, 56127 Pontedera, Italy
[2]Department of Excellence in Robotics and AI, Scuola Superiore Sant'Anna, 56127 Pisa, Italy
[3]Advanced Robotics Centre, National University of Singapore, Singapore 119077
[4]Department of Mechanical Engineering, National University of Singapore, Singapore 119077

Corresponding author: Daniele Somma (daniele.somma@santannapisa.it)

This work was supported in part by the European Union's Horizon 2020 Future and Emerging Technology (FET)-Open Program under Grant 863212 (PROBOSCIS Project); in part by Fondazione Pisa-Scientific and Technological Research (Soft Humanoid companion for motor Assessment and REhabilitation of children with Cerebral Palsy (SHARE-CP) Project) under Grant CUP J83C24000530007; in part by Ministero dell'Universita e 'della Ricerca (Italian Ministry of University and Research), Piano Nazionale Complementare (PNC), FIT4MEDROB "Fit4MedRob-Fit for Medical Robotics" Project under Grant PNC0000007; and in part by the Dextrous, strong yet soft robots (DESTRO) Project "Dextrous, Strong Yet Soft Robots," funded by Ministero degli Affari Esteri (MAE), Italy, and Agency for Science, Technology and Research (A*STAR), Singapore, under Grant R22I0IR124.

ABSTRACT This work presents a novel control strategy for the hand-guidance of a soft continuum arm. This promotes human-robot interaction in collaborative robotics; the proposed control system is implemented on a modular soft manipulator, exploiting its intrinsic safety. During hand guidance, users exert forces on the robot's end effector, which dynamically generates a smooth path for the robot to follow. A learning-based model is employed to predict the actuation patterns required to achieve desired positions, effectively solving the robot's inverse dynamics. The system's performance was evaluated under four distinct scenarios. In the human-guidance usability test, the controller demonstrated an average position error of 7.73 ± 0.96 mm. To validate robustness across different users, an inter-subject variability test with 10 participants yielded a consistent average error of 6.24 ± 3.05 mm. The system's resilience was further assessed in a noisy environment test, where the error remained bounded between 6.99 ± 3.40 mm and 34.64 ± 14.75 mm even under severe sensor degradation. Finally, under motor-driven guidance, the controller ensured accuracy across varying movement directions with an average position error of 3.82 ± 3.32 mm. These results underline the potential of soft robots for safe and interactive use in everyday environments, showcasing their suitability for collaborative applications.

INDEX TERMS Hand-guiding, human–robot interaction, neural networks, soft robotics.

I. INTRODUCTION

Hand guidance in robotics is a control method where a human operator directly manipulates the robot to guide it through a desired trajectory [1]. This interaction mode is widely used in industrial assembly [2], manufacturing [3], collaborative robots [4], and medical rehabilitation. These studies emphasize safety, operability, and human assistance, exploring different input devices like triaxial joysticks and force/torque sensors; methods like assisted gravity compensation [5] and Cartesian impedance control for redundant robots [6] have been proposed to enhance hand-guided systems' performance.

Traditional hand-guidance controllers have been applied predominantly on rigid robots, which excel in precision and repeatability but pose challenges in unstructured environments and human-robot collaborative settings due to their inherent stiffness and bulkiness. Addressing these concerns often involves complex sensor systems and advanced force control algorithms, increasing the system's cost and complexity without fully resolving the issue of limited compliance [7]. Differently from rigid robots, whose dynamics can be

The associate editor coordinating the review of this manuscript and approving it for publication was Thomas Canhao Xu.

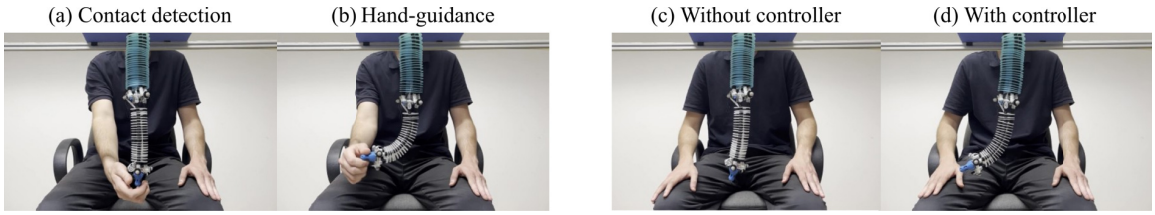

FIGURE 1. Hand-guidance soft continuum arm controller. (a) the user is touching the robot at its end-effector and the force sensor measures the force applied. (b) The user guides the robot towards a target position in space. If the controller is not working, only the soft manipulator's elasticity is exploited to move the robot. Instead, if the controller is working the force sensor translates the user's intention. The controller generates a new target position and the *Long-Short Term Memory*-based inverse dynamic model generates the actuation pattern to reach it. The effect of this controller is to actively move the robot in the direction imposed by the user, without any resistance. (c) In the case without the controller: once the force is removed, since the robot was not actuated, but only the softness of the material was exploited, the robot moves back to its equilibrium point (initial configuration) due to the gravity. (d) In the case with the controller: once the force is removed, the robot is actuated and then keeps the final position, until a new force is applied.

described analytically, soft robots exhibit complex, history-dependent behaviors that are hard to model explicitly. Soft robots, designed with compliant materials, offer an alternative for a safe interaction due to their mechanical properties [8]. This intrinsic compliance allows soft robots to interact with humans and objects [9].

Soft robots are particularly well-suited for applications such as physical rehabilitation [10]. Most of the existing literature focuses primarily on wearable devices [11], [12]. However, in the field of assistive robotics using soft robots, there are few examples where a manipulator is directly employed [13] and even fewer where it is controlled by a human.

Additionally, there is an increasing demand for innovative solutions to support the elderly in maintaining their independence and improving their quality of life [14], [15]. Assistive robots can play a crucial role in this context by providing physical assistance and monitoring health conditions. In this context, soft assistive robots offer a distinct advantage due to their intrinsic compliance, which ensures safety during physical interaction. The development of a robust hand-guidance method for soft manipulators represents a crucial technical step toward future healthcare applications, such as soft robotic showers [16], designed to assist elderly individuals and support their caregivers.

This paper presents the development and implementation of a controller for hand guidance in soft robotic systems, as represented in Fig. 1. By leveraging the intrinsic compliance of soft robots, the proposed solution overcomes the limitations of rigid robots. Our approach enhances the responsiveness of the robot to human input while ensuring safety during hand-guidance. The method was assessed for precision and motion smoothness, highlighting the potential of soft robotics to transform human-robot collaboration, especially in adaptive tasks and those where safety plays a critical role. The contributions of this work are the design of a novel controller for hand guidance in soft manipulators, which exploits the direct interaction with the user and its experimental validation, demonstrating reliable guidance despite passive compliance.

II. RELATED WORKS

Soft robots provide inherent safety during human interaction and exhibit adaptability in uncertain environments, making them well-suited for applications in healthcare [17] and home assistance [18]. These characteristics are essential for robots functioning in human-centric environments. However, controlling soft robots remain challenging due to their stochastic behavior [19], often stemming from the materials properties and manufacturing processes [20].

Various approaches have been proposed to address these challenges; one such class of methods involves machine learning (ML)-based models, valued for their ability to learn from real robot data, though stability is not guaranteed [21]. Reinforcement learning (RL)-based solutions [20] can develop inherently stable control strategies, though they require extended training periods and a simulated environment. In [22] and [23] soft robots were modeled by training an artificial neural network, showing good performance. In [24] the authors show that recurrent neural networks, such as Long-Short Term Memory (LSTM) produce estimates with errors that are 20% lower than the ones of the feedforward neural network trained with the same dataset.

Non-learning-based control methods, such as finite element methods, discrete differential geometry, or neural Ordinary Differential Equations (ODE)s, for soft robots present significant difficulties, primarily because designing controllers for systems with virtually infinite degrees of freedom is inherently challenging [25]. Moreover, these methods often require detailed physical modeling and are computationally expensive, whereas data-driven approaches, despite being robot-specific allow for easily generating a controller for a different soft arm by retraining on a new dataset without the need to define a new physical model, as shown in [24]. Most works focus on controlling the soft robot itself, with less attention given to how it interacts with its environment. Soft manipulators exhibit nonlinear and complex dynamics, further complicating control in unknown environments, where uncertainties such as sensor noise can exacerbate difficulties [26]. These factors limit the effectiveness of traditional control methods, as developing precise

analytical models often requires considerable assumptions or simplifications [27].

Most existing soft robot controllers emphasize position control and trajectory-following tasks [20], [24], [28], [29]. While recent studies have demonstrated the potential of soft robots in dynamic tasks beyond trajectory tracking [30], [31], few have concentrated on the interaction between users and soft robotic arms. In [18], a learning-based control method is proposed for force/position tracking in soft robot-environment interaction systems.

A hand-guided control method for soft continuum arms would enable robots to perform tasks in and around human environments, such as in healthcare or home assistance. However, there are very few studies demonstrating the control of soft robots through human interaction. This is mainly due to two key challenges: the process requires a sensing device to facilitate interaction between a soft robot and a human, and a controller able to transfer human intentions to the soft robots [32]. There are two different approaches to address these challenges: hardware-based [33], [34] solutions or teleoperation-based solutions [35], [36], [37], [38], [39], [40], [41]. In the first category, [33] presents a touchless human-soft robot interaction system based on flexible smart skin. The authors propose a distance control method that enables humans to control the 3D movements of soft robots interactively. In the second category, teleoperation-based systems can be further divided into those operating in a leader-follower configuration and those operating in a virtual environment. In [35], the movements of a traditional gaming joystick are mapped to the motions of a continuum robot, while other solutions, such as [36], leverage the capability of the leader device to achieve configurations identical to the continuum follower robot. Additionally, [37] and [38] introduce an intuitive approach for controlling the shape (configuration) of arbitrary 3D soft robots in a virtual environment. In this work, we address the sensing and control challenges through a physical hand-guided paradigm: the user interacts with the robot by applying forces directly to its end-effector (EE). These forces are measured and interpreted as expressions of movement intention. We then design a control strategy that maps these force inputs to actuator commands, accounting for the robot's nonlinear and compliant dynamics. This approach leverages the inherent compliance of soft robots to enable safe, intuitive, and natural human-robot interaction, without needing external leader devices (e.g. joysticks) or virtual interfaces, as in prior works.

III. MATERIALS AND METHODS

A. METHODOLOGY

Hand guidance requires the application of an external force on the EE of the robot and the precise knowledge of the dynamics of the robot, to make the system able to ''follow'' the external force. Our controller exploits the compliance of the soft manipulator, whose model is learned using a LSTM. This choice was motivated by the ability of LSTM networks to provide both accuracy, generalizability [24], real-time operation [42] and platform agnosticism (for more details see Appendix A). In the proposed control scheme, represented in Fig.2, the forces exerted during hand guidance are used to generate target points $\mathbf{x}_{k+1}$ in space, which are then fed into the inverse model to guide the robot's motion. The target point, for each timestep k is determined according to the current position $\mathbf{x}_k$, the external force $\mathbf{F}_{ext}$ and a gain factor k_p, according to (1)

$$\mathbf{x}_{k+1} = \mathbf{x}_k + k_p \mathbf{F}_{ext} \tag{1}$$

This method is particularly effective because it inherently exploits the soft manipulator's flexibility, allowing for smooth movements. This approach, based on combination of trajectory and force control, allows the system to handle interactions without requiring overly complex control schemes, making it a reliable yet straightforward solution.

The experimental evaluation was carried out in different scenarios. First, the effectiveness of the proposed controller was examined through direct interaction with users, in order to demonstrate its usability in laboratory conditions and practical contexts, testing the performance in noisy environments. Moreover, to strengthen the statistical reliability of the results, experiments were conducted with 10 subjects. Finally, a systematic characterization of the system was performed to validate its performance quantitatively.

B. EXPERIMENTAL SETUP

The experimental setup (Fig.3) comprises three main components: (I) a multi-segment robotic platform, which involved a sequence of the I-SUPPORT robotic arm [43]; (II) an actuation unit responsible for providing pressure signals to the platform; and (III) sensors, Motion Capture (MoCap) system with six cameras, which are used to track the position of the robot EE and midpoint in real-time. Additionally, a 6-axis force sensor (Touchence S50C1-WM155-K1-P6I) with a maximum range of 50N is utilized to detect physical contact between the robot and the user. This sensor provides input to the controller, allowing it to adapt based on the force exerted by the user, thereby facilitating a responsive and interactive control mechanism that adjusts to user interactions. The I-Support robotic arm is a pneumatically actuated, modular, soft manipulator. Three McKibben-like actuators are integrated into each module and are positioned at 120° intervals from each other. For this study, two modules have been connected with a plexiglass interface that had a width of 3 mm. The modules are oriented with a 60° offset relative to one another. The modules are tapered to minimize the overall system weight. The proximal module uses pairs of McKibben-like actuators, while the distal module employs single chambers. To control the pneumatic actuation of the robot, we used six proportional pressure micro regulator valves (Camozzi K8P-0-E522-0). The robotic arm is attached to an aluminum support frame and is oriented downwards to counteract the effects of gravity. The robot arm measures a total length of 411 mm and weighs 232.5 g when it is in its relaxed state. The six-axis force sensor communicates

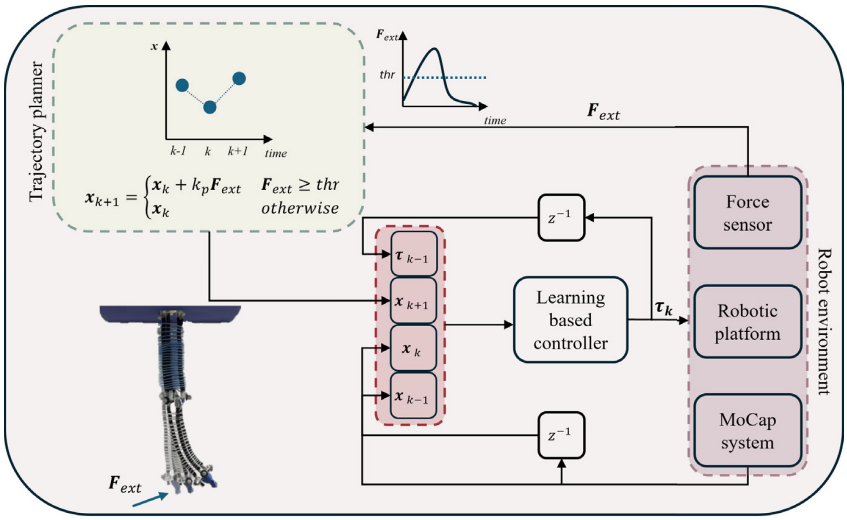

FIGURE 2. Hand-guidance learning-based controller. The strategy is based on generating a target point in space to be reached, resulting from the application of an external force to the soft robot's EE. The force information is converted into a new target position, considering the current position, direction, and magnitude of the force. Once the new target position, $\mathbf{x}_{k+1}$, is determined, it is combined with the current position $\mathbf{x}_k$, the previous position $\mathbf{x}_{k-1}$, and the current actuation state τ_k to create a new input for the learning-based controller. The controller then outputs the actuation command, τ_k, required to reach the target position, which is subsequently sent to the soft robotic platform.

with the computer using Inter-Integrated Circuit (I2C) bus communication; it measures the external force that is applied on the EE of the manipulator. On top of the sensor, we screwed a small 3D-printed small knob. It allows to easily move the robot by acting on its EE, and in particular, it facilitates the application of force to the sensor. To evaluate the system's precision in controlling the soft robotic arm regardless of movement direction, a DC motor (Dynamixel XM430-W210) was connected to the EE via a pulling cable. A plexiglass ring was attached to the robot's support structure to cover the workspace. This ring, which features holes spaced every 30°, was used to anchor the motor and ensure uniform coverage of the robot's workspace.

C. PROTOCOL

Ten participants were instructed to interact with the robot upon hearing the "Go" signal from a speaker. Informed consent was obtained from all participants prior to the experiment. Subjects were selected within the age range of 25 to 36 years, including both male and female participants. To avoid potential bias, only individuals without prior experience in the use of soft manipulators were recruited, and they were allowed to interact with the robot using whichever hand they preferred, regardless of their dominant hand. Subjects were allowed to move the robot at their preferred speed and towards randomly selected positions, making the input to the controller unstructured. The experimental protocol consisted of three phases.

- Teaching phase: the working principles of the system were explained, and the experimenter demonstrated the robot's workspace by selecting a region that encompassed all the points within the area highlighted in Fig. 4.
- Familiarization phase: participants were allowed to freely use the robot until they felt confident while interacting with it.
- Testing phase: the participants move the robot at a self-selected speed, towards random positions, completing a total of 10 target points.

D. DATASET COLLECTION

Data were collected at 20 Hz, with both modules actuated. The goal of this phase was to generate sufficient data to approximate the system's dynamic behavior using the learning-based model. To achieve this, the robot's workspace needed to be uniformly covered during the data collection process. According to the displacement of the chambers inside the robot, we actuated the robot in such a way to reproduce linear patterns. The generation of the training dataset has been achieved through an *oriented* motor babbling technique in which the robot has been randomly actuated, constrained to reproduce linear patterns at the EE level, to which random white noise has been overimposed; to avoid the step response of the robot we modulated this signal with a double ramp (forward and backward phase). To collect the dataset to train the learning-based model we used different seeds and different noise level. For every attempt, the position of the EE, the position the middle point, and actuation values were recorded. The dataset consists of 6310 samples and has been split to prevent overfitting: 75% of the data is allocated to the training set, and 25% to the validation set. The data distribution is shown in Fig.4. Finally, the workspace explored during the collection of training

data lies within the following volume: $(\Delta x, \Delta y, \Delta z) \rightarrow (196.18, 203.48, 65.00)$ mm.

E. INVERSE DYNAMIC MODEL

The challenge in modeling soft manipulators is due to their hyper-redundancy and the non-linearities of their materials [25], [27]. For these reasons, data-driven techniques have been applied to address this challenge. Given that, according to the theory of manipulator dynamics, the control input τ is a function of the manipulator's configuration space variables $\mathbf{x}$ and their derivatives $\dot{\mathbf{x}}, \ddot{\mathbf{x}}$:

$$\tau = f(\mathbf{x}, \dot{\mathbf{x}}, \ddot{\mathbf{x}}) \tag{2}$$

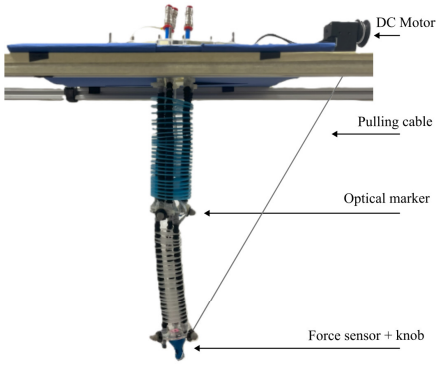

FIGURE 3. Experimental setup: optical markers are attached to the bimodular pneumatically actuated soft continuum manipulator to track the position of the EE and midpoint using a MoCap system. A force sensor is mounted on the EE, covered by a knob to facilitate user interaction. Additionally, a DC motor and a pulling cable are utilized to apply repeatable forces to the EE of the manipulator.

In (2) the velocity $\dot{\mathbf{x}}$ and the acceleration $\ddot{\mathbf{x}}$ can be discretized at a fixed discrete timestep ∂k, so the control input τ can be written as in (3)

$$\tau_k = f(\mathbf{x}_{k-2}, \mathbf{x}_{k-1}, \mathbf{x}_k, \delta k) \tag{3}$$

Assuming that δk remains constant when a fixed control frequency is selected, the system's dependence lies solely on the current task space variable and those from the previous two timesteps $\mathbf{x}_{k-2}, \mathbf{x}_{k-1}$. Starting from the aforementioned hypotheses, the inverse dynamic model of the soft robotic arm is reported in (4).

$$(\mathbf{x}_{k+1}, \mathbf{x}_k, \mathbf{x}_{k-1}, \tau_k) \longrightarrow \tau_{k+1} \tag{4}$$

As discussed in Section III-A a LSTM has been chosen to approximate 4 and a model selection is carried out to find the best combination of hyperparameters for our model. From (4) the training of the LSTM aims at finding at each timestep, given a future position $\mathbf{x}_{k+1}$ and the information needed to solve the kinematics of the manipulator, the actuation value τ_{k+1} to move the manipulator in $\mathbf{x}_{k+1}$. In designing the model, we chose to focus only on the horizontal plane components because of the design constraints of the robot, which prevent it from bending without stretching. This design-driven approach reduces control complexity by emphasizing the horizontal plane of motion, which is more relevant to the robot task space. Meanwhile, the vertical component is inherently derived from the robot motion and naturally aligns with its structural dynamics.

1) INVERSE DYNAMIC MODEL TRAINING

Both the task spaces and actuation spaces of the robot have been normalized in the range $[-1, +1]$. These data are used to train a model composed by an LSTM Cell and a feedforward linear output layer, whose hyperparameters were optimized by minimizing the *mean square error (MSE)*. The hyperparameters search space is reported in Table 1, and a grid search approach has been adopted. The model selection was based on the average error on the actuation components, while the hyperparameter search space was heuristically defined based on previous works [24]. To prevent overfitting, the dataset is first split into a training set (75%) and a validation set (25%), and then tested both offline on a separate, independent dataset and online on the robotic platform. The performance of the inverse dynamic model is evaluated during a trajectory-following task. The distribution of both the training and validation sets is shown in Fig.4.

TABLE 1. Model selection - Hyperparameters selection range and their best combination for the inverse dynamic model.

Hyperparameter	Range	Best model
Hidden size	16, 32, 64, 128	64
Epochs	100, 150, 200, 250, 300	150
Learning rate	$1e^{-2}$, $1e^{-3}$, $1e^{-4}$, $1e^{-5}$	$1e^{-2}$
Activation function	ReLU, Tanh, Sigmoid	ReLU

The final architecture consists of a single LSTM layer with 64 hidden units, followed by a fully connected layer to produce the actuation outputs. The network was trained for 150 epochs using the Adam optimizer, a learning rate of 10^{-2}, and the ReLU activation function. To prevent overfitting, early stopping was applied based on the validation loss, to ensure that the training process was stopped as soon as validation performance degraded. The training took approximately 7.9 seconds to train on a laptop with Python-based environment, a Windows 11 operating system, 16.0 GB RAM, and 11th Gen Intel(R) Core (TM) i7-11800H @ 2.30GHz.

This configuration corresponds to the best-performing entry in Table 1.

The model achieved a *MSE* on the validation set of $3.8 \cdot 10^{-3}$.

2) INVERSE DYNAMIC MODEL PERFORMANCE

The performances of the proposed model have been evaluated in the trajectory following task on the robotic platform. Linear trajectories with different movement directions and different over-imposed white noise have been predefined, and at each time step, the new target position has been provided as an input. Considering a given timestep k the model approximate the function reported in (5)

$$(\mathbf{x}_{k+1}, \hat{\mathbf{x}}_k, \hat{\mathbf{x}}_{k-1}, \hat{\tau}_k) \longrightarrow \hat{\tau}_{k+1} \tag{5}$$

According to (5) the robot is in position $\hat{\mathbf{x}}_k$, measured using MoCap and the model estimates $\hat{\tau}_{k+1}$ to move in the predefined target position $\mathbf{x}_{k+1}$. We tested the generalization and accuracy capabilities of the model, applying 10 different predefined trajectories and also its repeatability, by applying the same predefined input trajectory three different times. We got an average position error of the EE among the different trajectories of 8.21 ± 1.22 mm and an average *intra-trajectory* variability of 2.41 mm. The repeatability of the model is also affected by the mechanical properties of the soft arm [20]. These results are comparable with those present in the literature [19]. The average inference time of the network is 0.33 ± 0.47 ms, making the model suitable to control the system at 20 Hz.

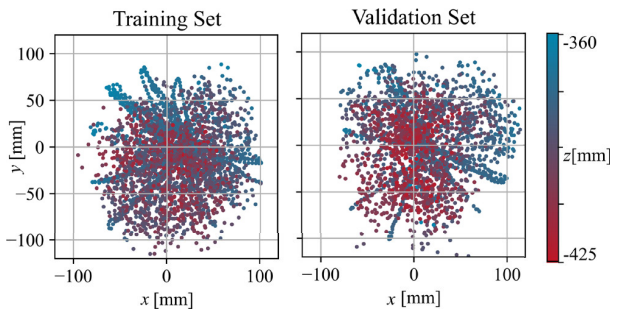

FIGURE 4. Workspace exploration. The trajectory of the EE is shown in the *xy* plane as a function of its *z*-coordinate. Data were collected by superimposing white noise onto the linear path of the EE at an actuation frequency of 20 Hz. The plots highlight the linear motion of the EE. The collected data were divided, with 25% used as a validation set to determine the optimal combination of hyperparameters for approximating the model described in (5).

IV. RESULTS

Our results indicate that the proposed control strategy allows the soft manipulator to be hand-guided with a final error of less than 10 mm. This property has been tested in all directions of the soft robot workspace. Experiments were conducted under two distinct conditions. In the *human-guided cases*, the robot was driven by users in order to evaluate its usability in both controlled laboratory settings and noisy environments, as well as to analyze inter-subject variability. In the *DC motor-guided case*, external forces were applied via a cable actuated by a DC motor.

The results can be quantitatively categorized as follows:

- **Position error**: it is defined as the distance between the position of the EE after the release of the force and the last target position, generated by the controller while applying external forces. Given the final time instant $t = t_f$, the position of the EE of the robot $\mathbf{x}_{ee}$ and the desired target position $\mathbf{x}_{des}$, the position error e_p is computed as reported in (6)

$$e_p = |\mathbf{x}_{ee} - \mathbf{x}_{des}|_2 \qquad t = t_f \tag{6}$$

- **Overshoot**: it is defined as the maximum peak of the oscillations around the final position $\mathbf{x}_{ee_f}$, once the EE is released by the user.

$$overshoot = \left|\max(\mathbf{x}_{ee}) - \mathbf{x}_{ee_f}\right|_2 \quad t_2 < t < t_3 \tag{7}$$

- **Smoothing ratio *(SR)***: it is defined as the ratio between the average jerk during hand guidance in the active case and the passive one.

$$SR = \frac{jerk_{active}}{jerk_{passive}} = \frac{(\partial^3 \mathbf{x}_{ee}/\partial t^3)_{active}}{(\partial^3 \mathbf{x}_{ee}/\partial t^3)_{passive}} \quad t_1 < t < t_2 \tag{8}$$

TABLE 2. Summary of the results - Comparison between passive and active case.

	Position Error [mm]	Overshoot [mm]	Smoothing Ratio
Hand Guided Case - Usability Test	7.73 ± 0.96	3.54 ± 0.67	1.08 ± 0.19
DC Motor Case	3.82 ± 3.32	2.07 ± 0.71	1.35 ± 0.30

A schematic representation of the two different experimental scenarios is shown in Fig.5(a) and in Fig.5(b).

A. HUMAN-GUIDED CASE

Three different tests were performed:

- *Case 1 - Usability Test:* the experimenter was moving the robot towards random positions to measure the feasibility of the proposed solutions. In this scenario, 10 target positions were selected. For each position, two consecutive trials were performed: in the first, the robot reached the target with the controller switched on, while in the second, it was guided back to the same position with the controller switched off. This procedure was repeated for all 10 positions, resulting in a total of 20 trials.
- *Case 2 - Noisy environment Test:* The experimenter moved the robot towards 10 randomly selected target positions. The test was repeated six times, each time simulating a different proprioceptive sensing noise band n_b. To reproduce noisy conditions beyond controlled laboratory settings, zero-mean Gaussian noise was added to the robot's position measurements. The standard deviation σ of the distribution was chosen such that $3\sigma = n_b$, ensuring that 99.7% of the noise values fall within the specified band. The tested noise bands were: [0, 5, 10, 20, 50, 100] mm.
- *Case 3 - Inter-Subject Variability Test:* This use case involves testing on different subjects. As mentioned in III-C, 10 subjects, after a teaching and demonstration phase, were asked to move the robot to 10 different random positions, to assess whether there was a significant degradation of performance when operated by different users.

1) USABILITY TEST

The performance of the controller is summarized in Table 2, which presents the evaluation metrics. The table indicates that the controller effectively responds to hand guidance from users, achieving an average position error of 7.73 ± 0.96 mm. Furthermore, the system exhibits oscillatory behavior around its final position,

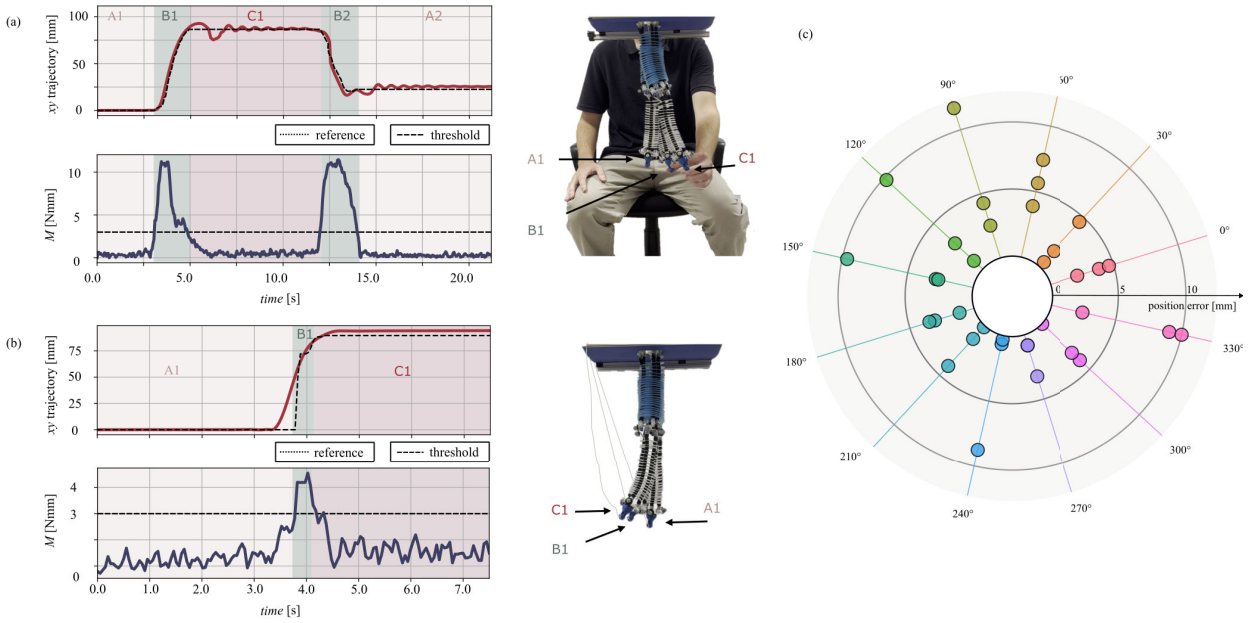

FIGURE 5. (a) Schematic representation of the Hand Guided Case - Usability Test: In A1, the robot begins in its initial configuration. In B1, it is hand-guided by the user toward the final position. In C1, the controller stabilizes the robot at the final position, with human-robot interactions illustrated in the top right. In B2, the user moves the robot back to its initial configuration, which is reached in region A2. (b) Schematic representation of the DC Motor Case: For each DC motor position, three trials were conducted to cover uniformly the entire workspace. A1 shows the robot in its initial configuration, while in B1, the DC motor moves the robot to the final position, and in C1, the controller stabilizes it. In B1, the cable is tensioned to pull the robot, while in C1, the cable is slack, indicating that no more forces are being applied to the end-effector. (c) Polar plot, which represents the position error (in the DC Motor Case) at different angles around a 360° plane. The plot illustrates that the position errors are not uniform across different directions. Some areas show larger errors (points further from the center), particularly near 330°. This indicates that the system has greater difficulty maintaining accuracy in these directions. Conversely, errors are smaller near angles like 210° and 270°, where points are closer to the center, indicating better positional accuracy. On average the positions errors are within the 5 mm region, indicating the low level of variability among trials. The average error is 3.82 ± 3.32 mm.

resulting in an overshoot of 3.54 ± 0.67 mm. Additionally, the measured SR is 1.08 ± 0.19 mm, suggesting that during the "hand-guidance" interval, denoted as B in Fig.5(a), the robot moved compliantly with the user. This test demonstrates the feasibility of the proposed solution.

2) NOISY ENVIRONMENT TEST

The performance of the controller is summarized in Fig.6, which shows the position error. The results show a progressive increase in both the mean error and variability as the noise level rises. As reported in Tab.3, the position error increased from 6.99 ± 3.40 mm in the case of no noise to 34.64 ± 14.75 mm in the case with a noise band of 100 mm.

3) INTER-SUBJECT VARIABILITY TEST

The performance of the controller was evaluated in an inter-subject variability test involving 10 participants to assess its effectiveness and generalizability. The comprehensive results are presented in Fig.7. The system achieved an average position error of 6.24 ± 3.05 mm across all subjects, indicating that the controller effectively accomplished the task. Moreover, this test confirms that the model is able to generalize over different trajectories and subjects, without overfitting the data.

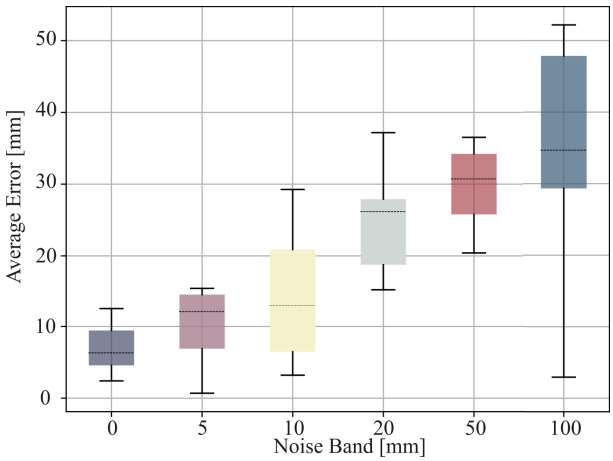

FIGURE 6. Noisy environments test - Boxplot of the average position error under different noise conditions. The noise band n_b represents three times the standard deviation σ of the Gaussian distribution from which the values are sampled, ensuring that with a 99.7% probability the values fall within this band.

B. DC MOTOR GUIDANCE

In this experiment we choose 12 directions, spaced 30° from one another and centered with the axis of the robot, to explore uniformly the EE workspace. For each direction three trials were completed resulting in a total of 72 trials,

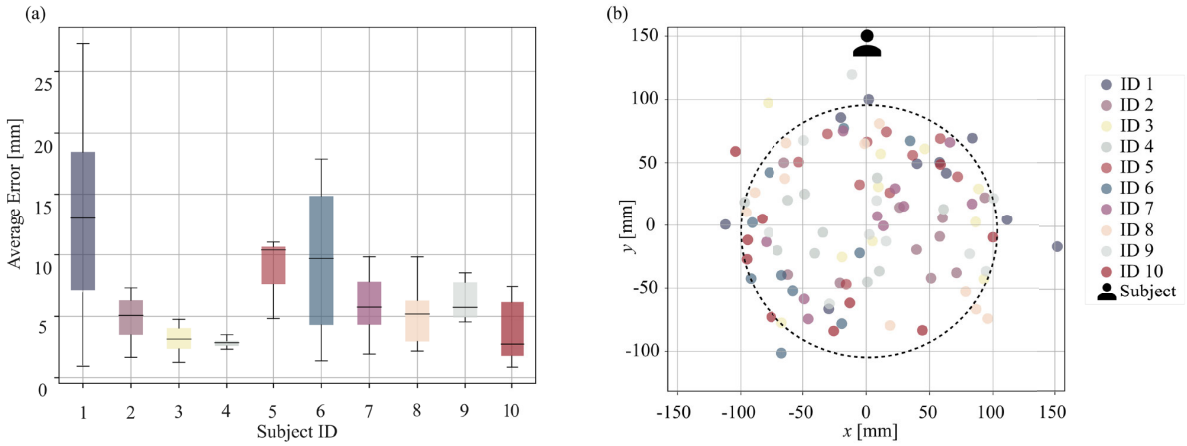

FIGURE 7. Inter-subject variability test - (a) shows the position errors obtained for the 10 subjects. (b) shows the distribution of points explored by each subject during the test. The dashed line represents the workspace that was highlighted by the experimenter during the teaching phase, considering the distribution of the training data in Fig.4.

TABLE 3. Summary of the results of the robustness tests.

Noise band [mm]	Average error [mm]
0	6.99 ± 3.40
5	10.18 ± 5.89
10	14.21 ± 8.76
20	24.86 ± 6.79
50	29.65 ± 5.46
100	34.64 ± 14.75

36 with the controller actively working and 36 without the controller, exploiting only the passive compliance of the soft manipulator. This use case is designed to assess the capability of the system to perform well, independently on the direction of movement. Indeed, removing the human interaction allows testing the controller systematically; the controller's performance is summarized in Table 4. These factors cannot be evaluated quantitatively during human interaction; The system demonstrated an average position error of 3.82 ± 3.32 mm. Moreover, as shown in Fig.5(b), once the cable is released and the force is no longer applied to the EE, the robot begins to oscillate around its final position, with an average overshoot of 2.07 ± 0.71 mm. The results further suggest that during the hand-guidance phase, the robot responds smoothly to the force exerted by the pulling cable, with an average SR of 1.35 ± 0.30. Table 4 presents the average position errors recorded for each of the 12 positions tested, while Fig.5(c) illustrates that although the controller effectively enables hand guidance in all directions, certain regions exhibit higher errors and overshooting.

V. DISCUSSION

The study presents a learning-based control strategy for hand-guided positioning of a soft robotic arm, evaluated in two distinct experimental scenarios. While the controller successfully enabled hand-guidance of the soft robot (as shown in the Supplementary material link), several important aspects need further exploration to understand the broader implications and potential limitations of this approach.

TABLE 4. DC motor case - Average results for each of the 12 positions of the DC motor.

Position ID	Error [mm]	Overshoot [mm]	Smoothness Ratio
0°	3.58 ± 1.03	2.76 ± 1.03	1.39 ± 0.07
30°	2.2 ± 1.72	3.21 ± 0.71	1.44 ± 0.07
60°	5.65 ± 1.44	1.21 ± 0.58	1.57 ± 0.48
90°	6.16 ± 3.97	4.00 ± 0.59	0.82 ± 0.14
120°	4.5 ± 3.81	1.17 ± 0.91	0.52 ± 0.24
150°	5.05 ± 3.24	1.30 ± 0.60	1.67 ± 0.22
180°	2.41 ± 0.91	1.58 ± 0.31	1.52 ± 0.58
210°	1.84 ± 1.64	1.71 ± 0.63	1.26 ± 0.13
240°	3.23 ± 3.9	2.72 ± 0.81	1.23 ± 0.64
270°	1.63 ± 1.14	0.45 ± 0.13	1.15 ± 0.26
300°	2.42 ± 1.72	1.13 ± 0.5	1.22 ± 0.50
330°	7.18 ± 3.35	3.62 ± 1.63	2.51 ± 0.30

A. NOISY ENVIRONMENT PERFORMANCE

The results show a monotonic increase in the average position error as the noise level grows, confirming the sensitivity of the controller to proprioceptive uncertainty. Up to a noise band of 10 mm, the system maintains a reasonable level of accuracy, suggesting that the controller can tolerate moderate disturbances without a substantial performance drop. Beyond 20 mm, however, the error increases, indicating a limitation in the controller's performance under high levels of sensor inaccuracy. The standard deviation also tends to increase with the noise amplitude, highlighting that not only does the mean performance degrade, but also the reliability of the controller becomes less predictable. These findings suggest that the controller can be effectively deployed in environments where proprioceptive sensing is noisy. Additionally, this test gives hints on the minimum accuracy requirements for the selection of the proprioceptive sensing modality.

B. INTER-SUBJECT VARIABILITY

The results show that the controller performs effectively across 10 different users, achieving an overall mean positional error of 6.24 ± 3.05 mm, thereby demonstrating reliable accuracy. While individual differences naturally

exist, all participants were able to successfully control the system, indicating its adaptability and ease of use. Fig.7(a) reports the distribution of average positional errors across participants, highlighting inter-subject variability. Fig.7(b) depicts the spatial regions explored by the subjects, and the workspace shown to the subjects during the teaching phase. Notably, Subject 1 exhibited the largest positional error, which can be primarily correlated to the fact that some of the selected positions were outside the workspace. To assess the robustness of the controller against user-specific variability, we conducted a statistical analysis on the error distributions collected from the 10 participants. Given the non-parametric nature of the error distribution, a Kruskal-Wallis H-test [44] was performed. The analysis revealed a statistically significant difference in performance among subjects ($H = 25.19, p = 0.0028$). This variability, visualized in Fig.7, is expected in human-in-the-loop scenarios, reflecting individual differences in manual dexterity and familiarity with the hand-guidance interface. However, from a practical standpoint, the system demonstrated operational robustness even in the worst-case scenario (Subject 1), whose accuracy remains well within the functional requirements for successful task execution.

C. COMPARISON BETWEEN THE TWO EXPERIMENTAL SCENARIOS

The experiments are divided into two cases: human-guidance and DC motor-guidance to apply forces to the manipulator. In the first case, the robot exhibited a higher positioning error compared to the second one. This difference is largely due to the inherent variability in human interaction, including inconsistencies in force application, speed, and motion paths. As shown in Fig. 5(c), certain directions (e.g., 330°, 90°) experienced larger errors, likely due to mechanical constraints, sensor limitations, or the control algorithm's performance in these directions. Although the three pairs of actuators are equally spaced around the circumference, some regions show slightly degraded performance, possibly due to mechanical asymmetries or manufacturing imperfections in the actuators. Another factor that strongly impacts learning-based models, as noted in [31], is the training data distribution. In this work, as described in Section III-D we generated the training date uniformly in the workspace; however, to mitigate these anisotropic errors, a possible strategy is to enrich the training dataset by oversampling trajectories in the directions where higher inaccuracies were observed, so that the model can better learn actuation patterns in those regions. In addition, direction-dependent gain tuning could be introduced at the control level to further compensate for mechanical or sensing asymmetries. While the second scenario demonstrates precision under ideal conditions, it does not capture the unpredictability of real-world scenarios, which is more accurately reflected when the user is involved. In both experimental cases, the system's smoothness was relatively low (1.08 in the Human-Guided Case vs. 1.35 in the DC Motor-Guided). As shown in Fig. 5(b) the applied force was more impulsive, resulting in a faster response from the robot and consequently a higher SR compared to the Human-Guided Case, in the usability test.

D. LIMITATIONS IN LEARNING-BASED CONTROL

While the learning-based controller demonstrated satisfactory performance, it operates within the limitations imposed by the quality of the training data. Soft robots exhibit highly nonlinear and complex dynamics, which can vary significantly depending on external factors (e.g., force direction, magnitude, interaction context). Although the inverse dynamics model based on LSTM produced promising results, with an average positioning error comparable to state-of-the-art solutions [19], further improvements could be made to enhance its ability to generalize to unseen environments and novel tasks. The stochastic nature of soft robots makes it challenging to create a comprehensive dataset that captures all possible variations in robot behavior, which in turn limits the adaptability of the model.

E. LIMITATIONS IN SENSING MODALITIES

The true potential of the proposed controller is currently hindered by its reliance on external sensing. While force sensors could still be realistically employed in real-world scenarios, the limited portability of MoCap systems significantly restricts the applicability of the controller and its deployment in unstructured environments, thereby narrowing the scope of human–soft manipulator interaction [45]. In the state of the art, different proprioceptive sensing technologies have been investigated as alternatives to external MoCap [46]. Resistive strain sensors [47], for example, can be integrated into flexible textiles to provide distributed measurements of deformation but may suffer from hysteresis and long-term drift, while optical approaches such as Fiber Bragg Grating sensors [48] offer high sensitivity and spatial resolution; they remain fragile, costly, and prone to error accumulation along the manipulator. Vision-based methods [49], while offering reliable performance, are heavily dependent on line-of-sight and controlled imaging conditions, such that even small occlusions or misdetections can trigger cascading errors along the manipulator body [50]. Overall, while external sensors offer reliable ground-truth in controlled settings, the long-term use of continuum soft manipulators will require hybrid onboard sensing strategies that combine complementary modalities to reduce errors, increase robustness, and ease calibration for real-world deployment [32].

VI. CONCLUSION

In this paper, we introduced a learning-based control method for hand-guided control of soft robots. The system shows satisfactory performance in controlled environments but also highlights several challenges, as explained in Section V.

A key limitation of the current approach is its reliance on external sensors, such as the MoCap system and force sensor. While these sensors are accurate in controlled settings, they may not be practical for widespread use due to their cost, complexity, bulkiness, and the need for

precise calibration in real-world applications. Additionally, some practical problems could arise from the use of these sensory modalities. The optical markers of the MoCap system could be occluded during the interaction, while the location of the force sensor determines the nature of the interaction. The system's robustness to real-world settings is supported by two key findings. First, the controller successfully handled the stochastic nature of human hand-guidance (unstructured input). Second, the noise injection tests demonstrated tolerance to severe sensor degradation (simulating real-world hardware constraints).

Similarly, in industrial settings, this control framework could enable safe collaborative manipulation. This approach holds significant potential for assistive robotics, where robots must work closely with humans in dynamic and unpredictable environments, such as in healthcare for physical rehabilitation or providing home assistance for the elderly. Furthermore, hand-guided control systems could greatly benefit robot teaching tasks. Through direct interaction, soft robots could learn new tasks, taught by human operators using "learning by demonstration" techniques. In conclusion, this work represents a valuable step forward in developing intuitive control systems for soft robots. It has the potential to greatly improve human-robot collaboration and open new opportunities in assistive and industrial applications. To address current limitations, future research will focus on integrating intrinsic multimodal sensing and developing algorithms for the real-time adaptation of the control policy to environmental uncertainties and robot dynamics variations, ensuring operational safety.

APPENDIX A
MODEL BENCHMARKING

To validate the architectural selection, the performance of the proposed LSTM was compared against baseline approaches: a static Feedforward Neural Network (MLP) and two RL agents: Proximal Policy Optimization (PPO) and Soft Actor-Critic (SAC). The proposed methods were evaluated and compared in terms of both training time and trajectory tracking accuracy on the forward model.

To train the RL agents, a learning-based forward model is required to simulate the environment. We used an LSTM-based forward model, since [24] shows that it has a lower error compared to other learning models. The hyperparameters of this forward model were optimized through a grid search exploring various neuron counts (16, 32, 64, or 128), learning rates ($1e^{-2}$, $1e^{-3}$, $1e^{-4}$, $1e^{-5}$), and activation functions (ReLU, tanh, sigmoid, or linear). The final optimal forward model consists of two layers with 64 neurons each, linear activations in both layers, and a learning rate of $1e^{-3}$.

To fairly compare the different approaches, LSTM and MLP were also trained on data gathered from the same forward model. The hyperparameters of the MLP were optimized by evaluating different combinations of hidden layers (1 or 2), neurons per layer (32, 64, 128, or 256), and activation functions (ReLU, tanh, or sigmoid). The optimal MLP configuration resulted in a single-layer architecture with 64 neurons and ReLU activation, as shown in Tab.5. The model selection for the LSTM is reported in Sec.III-E. To train the PPO agent, we replicated the procedure detailed in [51], while to train the SAC agent, we replicated the procedure detailed in [52].

TABLE 5. Model selection - Hyperparameters selection range and their best combination for the MLP.

Hyperparameter	Range	Best model
Hidden size	16, 32, 64, 128	64
Number of Layers	1, 2	1
Activation function	ReLU, Tanh, Sigmoid	ReLU

TABLE 6. Model selection - Hyperparameters selection range and their best combination for the forward model.

Hyperparameter	Range	Best model
Hidden size	16, 32, 64, 128	64
Learning Rate	$1e^{-2}$, $1e^{-2}$,$1e^{-4}$,$1e^{-5}$	$1e^{-3}$
Activation function	ReLU, Tanh, Sigmoid, Linear	Linear

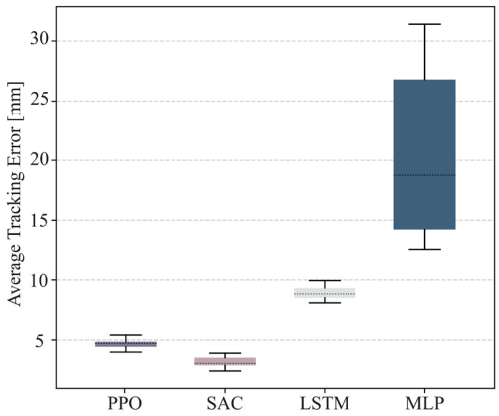

FIGURE 8. Model comparison. Boxplot of the average tracking error distribution when testing the inverse models on trajectory tracking, using the LSTM-forward model.

TABLE 7. Training time for the different models.

	Training Time [s]
PPO	$6.1 \cdot 10^3$
SAC	$4.1 \cdot 10^4$
LSTM	7.9
MLP	1.3

The MLP approach resulted in a significantly higher tracking error (22.25 mm). Conversely, while the RL agents achieved tracking accuracy (PPO: 4.66 mm, SAC: 3.16 mm) superior to the LSTM (8.92 mm), they demanded a disproportionately higher training time, as reported in Tab.7 and shown in Fig.8. Additionally, the RL approaches that seem to outperform others, when tested on a real robot, typically experience a drop in performance because they rely on training on the forward model. For instance, in [24], the error increases from 8.50 mm to 13.23 mm when the controller is deployed on the physical robot. In contrast,

the LSTM approach allows the model to be learned directly from real robot data, which leads to more robust and reliable performance. As shown in Sec.III-E, when the model is evaluated on the real robot in a trajectory-following task, it achieves an average position error of 8.21 mm, which is consistent with the result obtained when the LSTM is trained and tested on the forward model (8.92 mm). Moreover, the LSTM is better suited for long-term controller deployment, as it can be retrained quickly if the robot's behavior changes over time (e.g., due to variation in the robot's dynamics).

REFERENCES

[1] R. Balasubramanian, L. Xu, P. D. Brook, J. R. Smith, and Y. Matsuoka, "Physical human interactive guidance: Identifying grasping principles from human-planned grasps," *IEEE Trans. Robot.*, vol. 28, no. 4, pp. 899–910, Aug. 2012.

[2] M. Fujii, H. Murakami, and M. Sonehara, "Study on application of a human-robot collaborative system using hand-guiding in a production line," *IHI Eng. Rev.*, vol. 49, no. 1, pp. 24–29, 2016.

[3] M. Safeea and P. Neto, "Precise positioning of collaborative robotic manipulators using hand-guiding," *Int. J. Adv. Manuf. Technol.*, vol. 120, nos. 7–8, pp. 5497–5508, Jun. 2022.

[4] J. E. Solanes, L. Gracia, P. Muñoz-Benavent, J. V. Miro, M. G. Carmichael, and J. Tornero, "Human–robot collaboration for safe object transportation using force feedback," *Robot. Auto. Syst.*, vol. 107, pp. 196–208, Sep. 2018.

[5] C. Emmerich, A. Nordmann, A. Swadzba, J. J. Steil, and S. Wrede, "Assisted gravity compensation to cope with the complexity of kinesthetic teaching on redundant robots," in *Proc. IEEE Int. Conf. Robot. Autom.*, May 2013, pp. 4322–4328.

[6] J. Vogel, S. Haddadin, B. Jarosiewicz, J. D. Simeral, D. Bacher, L. R. Hochberg, J. P. Donoghue, and P. van der Smagt, "An assistive decision-and-control architecture for force-sensitive hand–arm systems driven by human–machine interfaces," *Int. J. Robot. Res.*, vol. 34, no. 6, pp. 763–780, May 2015.

[7] A. Bicchi, M. Bavaro, G. Boccadamo, D. De Carli, R. Filippini, G. Grioli, M. Piccigallo, A. Rosi, R. Schiavi, S. Sen, and G. Tonietti, "Physical human-robot interaction: Dependability, safety, and performance," in *Proc. 10th IEEE Int. Workshop Adv. Motion Control*, Mar. 2008, pp. 9–14.

[8] D. Rus and M. T. Tolley, "Design, fabrication and control of soft robots," *Nature*, vol. 521, no. 7553, pp. 467–475, May 2015.

[9] X. Li, D. Fan, Y. Sun, L. Xu, D. Li, B. Sun, S. Nong, W. Li, S. Zhang, B. Hu, and M. Li, "Porous magnetic soft grippers for fast and gentle grasping of delicate living objects," *Adv. Mater.*, vol. 36, no. 44, Nov. 2024, Art. no. 2409173.

[10] C.-Y. Chu and R. M. Patterson, "Soft robotic devices for hand rehabilitation and assistance: A narrative review," *J. NeuroEng. Rehabil.*, vol. 15, no. 1, pp. 1–14, Dec. 2018.

[11] E. Q. Yumbla, Z. Qiao, W. Tao, and W. Zhang, "Human assistance and augmentation with wearable soft robotics: A literature review and perspectives," *Current Robot. Rep.*, vol. 2, no. 4, pp. 1–15, Dec. 2021.

[12] C. Walsh, "Human-in-the-loop development of soft wearable robots," *Nature Rev. Mater.*, vol. 3, no. 6, pp. 78–80, May 2018.

[13] Y. Ansari, M. Manti, E. Falotico, Y. Mollard, M. Cianchetti, and C. Laschi, "Towards the development of a soft manipulator as an assistive robot for personal care of elderly people," *Int. J. Adv. Robotic Syst.*, vol. 14, no. 2, Mar. 2017, Art. no. 1729881416687132.

[14] T. Bock, C. Georgoulas, and T. Linner, "Towards robotic assisted hygienic services: Concept for assisting and automating daily activities in the bathroom," *Gerontechnology*, vol. 11, no. 2, p. 362, Jun. 2012.

[15] D. Dorling, "World population prospects at the UN: Our numbers are not our problem?" in *The Struggle for Social Sustainability*. Bristol, U.K.: Policy Press, 2021, pp. 129–154.

[16] A. Zlatintsi, "I-support: A robotic platform of an assistive bathing robot for the elderly population," *Robot. Auto. Syst.*, vol. 126, Apr. 2020, Art. no. 103451.

[17] M. Cianchetti, C. Laschi, A. Menciassi, and P. Dario, "Biomedical applications of soft robotics," *Nature Rev. Mater.*, vol. 3, no. 6, pp. 143–153, May 2018.

[18] Z. Tang, W. Xin, P. Wang, and C. Laschi, "Learning-based control for soft robot–environment interaction with force/position tracking capability," *Soft Robot.*, vol. 11, no. 5, pp. 767–778, Oct. 2024.

[19] E. Falotico, E. Donato, C. Alessi, E. Setti, M. S. Nazeer, C. Agabiti, D. Caradonna, D. Bianchi, F. Piqué, Y. T. Ansari, and M. Killpack, "Learning controllers for continuum soft manipulators: Impact of modeling and looming challenges," *Adv. Intell. Syst.*, vol. 7, no. 2, Feb. 2025, Art. no. 2400344.

[20] M. S. Nazeer, C. Laschi, and E. Falotico, "RL-based adaptive controller for high precision reaching in a soft robot arm," *IEEE Trans. Robot.*, vol. 40, pp. 2498–2512, 2024.

[21] D. Kim, S.-H. Kim, T. Kim, B. B. Kang, M. Lee, W. Park, S. Ku, D. Kim, J. Kwon, L. Ho-Chang, J. Bae, Y. Park, K. Cho, and S. Jo, "Review of machine learning methods in soft robotics," *PLoS ONE*, vol. 16, no. 2, 2021, Art. no. e0246102.

[22] T. G. Thuruthel, E. Falotico, F. Renda, and C. Laschi, "Learning dynamic models for open loop predictive control of soft robotic manipulators," *Bioinspiration Biomimetics*, vol. 12, no. 6, Oct. 2017, Art. no. 066003.

[23] M. T. Gillespie, C. M. Best, E. C. Townsend, D. Wingate, and M. D. Killpack, "Learning nonlinear dynamic models of soft robots for model predictive control with neural networks," in *Proc. IEEE Int. Conf. Soft Robot. (RoboSoft)*, Apr. 2018, pp. 39–45.

[24] A. Centurelli, L. Arleo, A. Rizzo, S. Tolu, C. Laschi, and E. Falotico, "Closed-loop dynamic control of a soft manipulator using deep reinforcement learning," *IEEE Robot. Autom. Lett.*, vol. 7, no. 2, pp. 4741–4748, Apr. 2022.

[25] T. G. Thuruthel, Y. Ansari, E. Falotico, and C. Laschi, "Control strategies for soft robotic manipulators: A survey," *Soft Robot.*, vol. 5, no. 2, pp. 149–163, Apr. 2018.

[26] J. Wang and A. Chortos, "Control strategies for soft robot systems," *Adv. Intell. Syst.*, vol. 4, no. 5, May 2022, Art. no. 2100165.

[27] C. Laschi, T. G. Thuruthel, F. Lida, R. Merzouki, and E. Falotico, "Learning-based control strategies for soft robots: Theory, achievements, and future challenges," *IEEE Control Syst.*, vol. 43, no. 3, pp. 100–113, Jun. 2023.

[28] T. G. Thuruthel, E. Falotico, M. Manti, and C. Laschi, "Stable open loop control of soft robotic manipulators," *IEEE Robot. Autom. Lett.*, vol. 3, no. 2, pp. 1292–1298, Apr. 2018.

[29] T. G. Thuruthel, E. Falotico, F. Renda, and C. Laschi, "Model-based reinforcement learning for closed-loop dynamic control of soft robotic manipulators," *IEEE Trans. Robot.*, vol. 35, no. 1, pp. 124–134, Feb. 2019.

[30] D. A. Haggerty, M. J. Banks, E. Kamenar, A. B. Cao, P. C. Curtis, I. Mezić, and E. W. Hawkes, "Control of soft robots with inertial dynamics," *Sci. Robot.*, vol. 8, no. 81, p. 6864, Aug. 2023.

[31] D. Bianchi, G. Campinoti, C. Comitini, C. Laschi, A. Rizzo, A. M. Sabatini, and E. Falotico, "SoftSling: A soft robotic arm control strategy to throw objects with circular run-ups," *IEEE Robot. Autom. Lett.*, vol. 9, no. 10, pp. 8250–8257, Oct. 2024.

[32] C. Hegde, J. Su, J. M. R. Tan, K. He, X. Chen, and S. Magdassi, "Sensing in soft robotics," *ACS Nano*, vol. 17, no. 16, pp. 15277–15307, 2023.

[33] W. Liu, Y. Duo, J. Liu, F. Yuan, L. Li, L. Li, G. Wang, B. Chen, S. Wang, H. Yang, Y. Liu, Y. Mo, Y. Wang, B. Fang, F. Sun, X. Ding, C. Zhang, and L. Wen, "Touchless interactive teaching of soft robots through flexible bimodal sensory interfaces," *Nature Commun.*, vol. 13, no. 1, p. 5030, Aug. 2022.

[34] F. Piqué, F. Stella, J. Hughes, E. Falotico, and C. D. Santina, "Smell driven navigation for soft robotic arms: Artificial nose and control," in *Proc. IEEE Int. Conf. Soft Robot. (RoboSoft)*, Apr. 2023, pp. 1–7.

[35] M. C. Yip and D. B. Camarillo, "Model-less feedback control of continuum manipulators in constrained environments," *IEEE Trans. Robot.*, vol. 30, no. 4, pp. 880–889, Aug. 2014.

[36] C. G. Frazelle, A. Kapadia, and I. Walker, "Developing a kinematically similar master device for extensible continuum robot manipulators," *J. Mech. Robot.*, vol. 10, no. 2, Apr. 2018, Art. no. 025005.

[37] J. M. Bern, W. C. May, A. Osborn, F. Stella, S. Zargarzadeh, and J. Hughes, "A soft robot inverse kinematics for virtual reality," in *Proc. IEEE Int. Conf. Robot. Autom. (ICRA)*, May 2024, pp. 14957–14963.

[38] Z. Liao, W. Wei, L. Zhang, Y. Gao, and Y. Cai, "An augmented reality-enabled digital twin system for reconfigurable soft robots: Visualization, simulation and interaction," *Comput. Ind.*, vol. 168, Jun. 2025, Art. no. 104285.

[39] A. Amaya, D. D. K. Arachchige, J. Grey, and I. S. Godage, "Evaluation of human-robot teleoperation interfaces for soft robotic manipulators," in *Proc. 30th IEEE Int. Conf. Robot Hum. Interact. Commun. (RO-MAN)*, Aug. 2021, pp. 412–417.

[40] F. Stroppa, M. Luo, K. Yoshida, M. M. Coad, L. H. Blumenschein, and A. M. Okamura, "Human interface for teleoperated object manipulation with a soft growing robot," in *Proc. IEEE Int. Conf. Robot. Autom. (ICRA)*, May 2020, pp. 726–732.
[41] B. T. Phillips, K. P. Becker, S. Kurumaya, K. C. Galloway, G. Whittredge, D. M. Vogt, C. B. Teeple, M. H. Rosen, V. A. Pieribone, D. F. Gruber, and R. J. Wood, "A dexterous, glove-based teleoperable low-power soft robotic arm for delicate deep-sea biological exploration," *Sci. Rep.*, vol. 8, no. 1, p. 14779, Oct. 2018.
[42] Z. Chen, M. Bernabei, V. Mainardi, X. Ren, G. Ciuti, and C. Stefanini, "A novel and accurate BiLSTM configuration controller for modular soft robots with module number adaptability," *Soft Robot.*, Dec. 2024, doi: 10.1089/soro.2024.0015.
[43] M. Manti, A. Pratesi, E. Falotico, M. Cianchetti, and C. Laschi, "Soft assistive robot for personal care of elderly people," in *Proc. 6th IEEE Int. Conf. Biomed. Robot. Biomechatronics (BioRob)*, 2016, pp. 833–838.
[44] W. H. Kruskal and W. A. Wallis, "Use of ranks in one-criterion variance analysis," *J. Amer. Stat. Assoc.*, vol. 47, no. 260, pp. 583–621, Dec. 1952.
[45] L. Wang, J. Lam, X. Chen, J. Li, R. Zhang, Y. Su, and Z. Wang, "Soft robot proprioception using unified soft body encoding and recurrent neural network," *Soft Robot.*, vol. 10, no. 4, pp. 825–837, Aug. 2023.
[46] G. Caroleo, A. Albini, and P. Maiolino, "Soft robot localization using distributed miniaturized time-of-flight sensors," in *Proc. IEEE 8th Int. Conf. Soft Robot. (RoboSoft)*, Apr. 2025, pp. 1–6.
[47] N. Pagliarani, C. Alessi, L. Arleo, G. Campinoti, M. Maselli, E. Falotico, and M. Cianchetti, "SoftTex: Soft robotic arm with learning-based textile proprioception," *IEEE Robot. Autom. Lett.*, vol. 10, no. 4, pp. 3779–3786, Apr. 2025.
[48] K. C. Galloway, Y. Chen, E. Templeton, B. Rife, I. S. Godage, and E. J. Barth, "Fiber optic shape sensing for soft robotics," *Soft Robot.*, vol. 6, no. 5, pp. 671–684, Oct. 2019.
[49] H. Zheng, S. Pinzello, B. G. Cangan, T. J. K. Buchner, and R. K. Katzschmann, "Vision-based online key point estimation of deformable robots," *Adv. Intell. Syst.*, vol. 6, no. 10, Oct. 2024, Art. no. 2400105.
[50] X. Chen, X. Zhang, Y. Huang, L. Cao, and J. Liu, "A review of soft manipulator research, applications, and opportunities," *J. Field Robot.*, vol. 39, no. 3, pp. 281–311, May 2022.
[51] C. Alessi, H. Hauser, A. Lucantonio, and E. Falotico, "Learning a controller for soft robotic arms and testing its generalization to new observations, dynamics, and tasks," in *Proc. IEEE Int. Conf. Soft Robot. (RoboSoft)*, Apr. 2023, pp. 1–7.
[52] M. S. Nazeer, D. Bianchi, G. Campinoti, C. Laschi, and E. Falotico, "Policy adaptation using an online regressing network in a soft robotic arm," in *Proc. IEEE Int. Conf. Soft Robot. (RoboSoft)*, Apr. 2023, pp. 1–7.

DANIELE SOMMA (Graduate Student Member, IEEE) received the B.Sc. degree in electronics engineering from the Polytechnic University of Bari, in 2020, and the M.Sc. degree in bionics engineering from the University of Pisa, in 2023. He is currently pursuing the Ph.D. degree in biorobotics with The BioRobotics Institute, Scuola Superiore Sant'Anna. He is a member of the BRAinInspired Robotics (BRAIR) Laboratory. His research focuses on the development of learning-based control algorithms for soft robotic systems in interactive tasks.

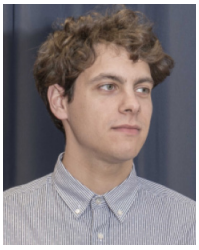

DIEGO BIANCHI (Student Member, IEEE) received the M.Sc. degree in mechanical engineering from the University of L'Aquila, in 2021. He is currently pursuing the Ph.D. degree with The BioRobotics Institute, Scuola Superiore Sant'Anna, Pisa, Italy. His research focuses on the development of learning-based control algorithms and the design of soft robotic systems.

FRANCESCO IORI received the B.Sc. degree in mechanical engineering and the M.Sc. degree in robotic and automation engineering from the University of Pisa, in 2018 and 2020, respectively. He is currently pursuing the Ph.D. degree in biorobotics with The BioRobotics Institute, Scuola Superiore Sant'Anna. He has been a member of the BRAinInspired Robotics (BRAIR) Laboratory, since 2021, after a year of work as a Research Assistant. From 2014 to 2020, he was an Honor Student with Scuola Superiore Sant'Anna, where he received the 2nd-level master's in industrial and information engineering. He is collaborating on the European projects HBP and APRIL, developing adaptive trajectory generation for unstructured handovers and learning-based motion planning. His research interest is in the application of predictive models to robot control.

CECILIA LASCHI (Fellow, IEEE) received the degree in computer science from the University of Pisa, Pisa, Italy, the Ph.D. degree in robotics from the University of Genoa, Genoa, Italy, and the Honorary Doctorate degree from the University of Southern Denmark, Odense, Denmark, in 2023. She is currently the Provost's Chair Professor of robotics with the National University of Singapore, Singapore, leading the Soft Robotics Laboratory. She is also the Co-Director of CARTIN–Centre for Advanced Robotics Technology and Innovation, Pisa. She was a JSPS Visiting Researcher with the Humanoid Robotics Institute, Waseda University, Tokyo, Japan. She is best-known for her research in soft robotics, an area that she pioneered and contributed to developing at an international level. She investigates fundamental challenges for building robots with soft materials, with a bioinspired approach that started with a study of the octopus as a model for robotics. She explores marine applications of soft robots and their use in the biomedical field, with a focus on eldercare. She founded the IEEE International Conference on Soft Robotics (RoboSoft). She is the Co-Chair of the Gordon Research Conference on Robotics 2024. She co-founded the spin-off company RoboTech. She is the Editor-in-Chief of *Bioinspiration and Biomimetics*, and the Specialty Chief Editor of Soft Robotics in *Frontiers in Robotics and AI* and an Editorial Board Member of Science Robotics and IEEE Robotics and Automation Letters.

EGIDIO FALOTICO (Member, IEEE) received the degree in computer sciences from the University of Pisa, Pisa, Italy, in 2008, and the Ph.D. degree in biorobotics with Scuola Superiore Sant'Anna (SSSA), Pisa, in 2013, and the Ph.D. degree in cognitive sciences from the University Pierre et Marie Curie, Paris, France, in 2013. He is currently an Assistant Professor with The BioRobotics Institute, SSSA, Pontedera, Italy. He is the author or co-author of more than 100 international peer-reviewed articles and he regularly serves as a reviewer for more than ten international ISI journals. He served as PI for SSSA in EU-funded projects (Human Brain Project, Proboscis, and Growbot), focusing on the development of brain-inspired algorithms for robot control and on machine learning models for soft robot control. His research interests focus on neurorobotics, i.e., the implementation of brain models from neuroscience in robots.